ICSV13 - Vienna
The Thirteenth International Congress on Sound and Vibration
Vienna, Austria, July 2-6, 2006

SOUND GENERATION BY FREE SURFACE PIERCING CYLINDERS

Eldad J. Avital*[1], Guangxu Yu[1] and John Williams[1]

[1]Department of Engineering, Queen Mary, University of London
Mile End Road, E1 4NS London, United Kingdom
e.avital@qmul.ac.uk

Abstract

Sound generation by a vertically mounted circular cylinder piercing free surface, is studied computationally using the Large Eddy Simulation and the acoustic analogy approaches for shallow water. The flow is simulated using the two-phase approach where both air and water phases are simulated. The interface surface is allowed to move and is simulated using the VOF technique. The resulted pressure distribution along the cylinder is used to calculate the dipole-generated sound propagation inside the water. The Lighthill-Curle acoustic analogy is reformulated to account for the interface surface which is modelled as a zero pressure surface. Hydrodynamic results are produced for a moderate sub-critical Reynolds number and a Froude number close to one, showing fair to good qualitative agreement with known results. However, sensitivity is found to the inflow condition, affecting the far field noise level. Nevertheless, a general pattern is revealed, showing the interface surface acting as a damper to shedding of vortex rollers under the water and also acting as a high pass filter for the underwater radiative modes. Thus the underwater far field sound is limited to frequencies much higher than the cylinder's fundamental shedding frequency and most of the sound emission and propagation is concentrated near the bottom floor.

INTRODUCTION

Free surface piercing cylinders are of great interest to marine engineering due to their relevance to off-shore structures, costal defenses and underwater vessels. In addition to the usual vortex shedding expected from a 2D cylinder, the free surface introduces a 3D effect that causes a variation in the force acting on the cylinder and the wake characteristics. The latter is bound to have an effect on the sound generation due to the interaction of the flow with the cylinder. This work focuses on the circular cylinder of a moderate sub-critical Reynolds number ($Re_D \cong 30 \cdot 10^3$), i.e. the boundary layer over the cylinder is laminar and the turbulence develops in the wake. Innoue et al.

[1] found experimentally that for shallow water the free surface wake attenuates the periodic vortex shedding and high frequency components. This was confirmed by the free surface incompressible Large Eddy Simulation (LES) of Kawamura et al. [2], where periodic vortex shedding (Von Karman rollers) was found only very close to the floor, which was in an ambient depth of 4*D* (*D* is the diameter of the cylinder).

The investigation of sound generation due to flow interaction with a solid circular cylinder goes back to the early days of aeroacoustics, where Powell [3] used his vortex sound theory to look at aelion noise. However, pressure surface source modelling as the Lighthill-Curle's formulation also proved to be popular due to its relatively easy computational implementation. Kato et al. [4] used such a formulation coupled with incompressible LES to achieve good agreements with measured results for low speed flows. Recently attention has been directed towards the near sound field [5] and further exploration of the Curle's surface formulation [6].

In this study will look at the effect the free surface has on sound emission and propagation. The latter are of importance for underwater vessel detection and sound-structure interaction. The incompressible LES approach will be used to simulate the flow evolution using the two-phase approach, i.e. both water and air flows are simulated. The Lighthill-Curle's surface formulation will be reformulated to account for the non-compactness in the vertical direction caused by the interface surface between the water and air phases. Attention will be directed towards the underwater sound propagation and thus the sound field propagation in the air phase will not be investigated in this study.

HYDRODYNAMIC FORMULATION

The fluid flow is taken as composed of two phases, water and air, with a clearly determined moving interface surface separating them. Both phase flows are taken as incompressible and governed by the two-phase Navier-Stokes (N-S) equations formulated on a curvilinear orthogonal grid;

$$\nabla \cdot \vec{V} = 0\,,\ \frac{\partial \vec{V}}{\partial t} + \left(\vec{V} \cdot \nabla\right)\vec{V} = -\frac{\nabla p}{\rho} + \frac{1}{\rho}\nabla \times \left[\mu\left(\nabla \times \vec{V}\right)\right]. \qquad (1)$$

The equations are discretised using a finite volume approach of a staggered grid and are simulated using the LES method as implemented in our in-house code *Lithium.*

The standard Smagorinsky model (*Cs*=0.2) with the Van-driest damping wall function was used to model the small scale contribution along with a second order *Quick* scheme for the convective terms as in [2]. The diffusion terms were calculated using a second order central scheme. The N-S equations were marched in time using the projection method and a third order Runge-Kutta scheme. The pressure equation resulting from the projection method was discretised using a second order central finite volume scheme and solved using the Preconditioned Bi-Conjugate Gradient Stabilized (PBCGSTAB) method along with a polynomial preconditioner [7].

The evolution of the interface surface between the air and water phases was

simulated using the VOF approach, where in this study the FCT-VOF method [8] was used to simulate the governing equation

$$\partial C/\partial t + \nabla\left(C\vec{V}\right)=0. \quad (2)$$

C is the relative concentration of the water phase in the finite volume cell. The local density and viscosity coefficients are approximated as follows

$$\rho = \rho_{water}C' + \rho_{air}\left(1-C'\right), \quad \mu = \mu_{water}C' + \mu_{air}\left(1-C'\right). \quad (3)$$

C' is a spatially filtered C using the local value and of the surrounding cells. It was found to accelerate the pressure solution while having little effect on the flow field behaviour. Higher order formulations as the PLIC are available, however for our needs and range of Froude numbers the current scheme was found to be sufficient.

A cylindrical co-ordinate system was used to capture the circular cylinder geometry, see Figure 1. No slip velocity wall conditions were imposed on the cylinder and free slip on the floor of the computational domain. On the outer radial edge, a velocity inflow disturbance of synthetic turbulent [9] and a single frequency disturbance with a spatially randomized phase were used. The frequency was chosen to be of St_D = 0.2 to encourage vortex shedding and thus reducing the computational time required to reach that stage. At the outlet, simple zero gradient conditions were used for the velocity field. Therefore a buffer zone was used in front of it, replacing gradually the convective term scheme to a 1st order upwind. Zero gradient boundary condition was also used for the colour C on the cylinder's wall and the outer radial edge. Thus a buffer zone was also used for C by adding gradually a body force to equ. (2), damping C back to its ambient value. Zero pressure condition was used at the top of the computational domain to model the effect of the ambient air pressure and to allow for air entrainment. Free slip conditions for the tangential velocities were used at the plane.

AEROACOUSTIC FORMULATION

The Lighthill-Curle acoustic analogy formulation was used to calculate the emitted sound by the cylinder. Due to the typically low Mach number in underwater acoustics, quadrupoles (volume momentum) sources were neglected and thus only dipole (force) source types generated by the forces acting on the cylinder were taken into account. Due the large impedance difference between the water and air phases the interface surface can be modelled as a zero pressure surface for the underwater sound propagation leading to a possible non-compactness in the vertical direction. Starting from Lighthill-Curle's equation [10], one gets

$$\partial^2\left(\rho'\cdot H\right)/\partial t^2 - c_0^2\nabla^2\left(\rho'\cdot H\right) = -\partial\left[F_i\delta(S)\right]/\partial x_i \; ; 0 \le x_3 \le h, \quad (4)$$

$$\partial\rho'/\partial x_3 = 0 \text{ at } x_3 = 0 \; ; \quad \rho' = 0 \text{ at } x_3 = h, \quad (5)$$

H is the Heaviside function that is zero inside the cylinder and one outside. x_3=0 is the floor and x_3=h is the interface surface which is assumed to be fixed. Thus the effect of the motion of the interface surface comes about only through the force distribution along the cylinder, i.e. the right hand side of Equ. (4).

Equations (4) & (5) can be solved in the Fourier space domain using the Fourier transform

$$\rho' = \sum_{m,n} \hat{\rho}_{mn} \cos(k_m x_3) e^{j\omega_n t} \; ; \quad k_m \equiv \frac{(2m+1)\pi}{2h}, \tag{6}$$

leading to the Helmholtz equation

$$\nabla_h^2 \hat{\rho}_{mn} + \hat{k}_{mn}^2 \hat{\rho}_{mn} = \frac{1}{c_0^2} \frac{\partial}{\partial x_h} \left[\hat{F}_h \delta(S) \right]; \quad \hat{k}_{mn}^2 \equiv \frac{\omega_n^2}{c_0^2} - k_m^2. \tag{7}$$

The suffix *h* stands for the horizontal rectangular directions 1 and 2. The fundamental solution of Equ. (7) is the first Hankel function that satisfies the radiation (Sommerfield) condition. Using the divergence theorem and integration by parts one can show that the acoustic power output *P* can be written as

$$P = \frac{1}{8\pi c_0 \rho_0} \int_0^h dy_3 \int_0^{2\pi} \sum_{mn} \hat{k}_{mn} \left(Fx_{mn} \cos\theta + Fy_{mn} \sin\theta \right)^2 d\theta, \tag{8}$$

where only radiative modes (positive $\hat{k}_{mn}^2$) are taken into account. *Fx* is the pressure drag force and *Fy* is the lift force acting on the cylinder, meaning as in the original Curle's expression the viscous stress effect is neglected [10]. The inner integrand in Expression (8) will be taken as the directivity at a certain height (y_3) and when averaged over y_3 will be the overall directivity $D(\theta)$. The frequency density spectrum will be the inner integral at a fixed frequency *n* and the overall one is averaged over y_3. In practice the aeroacoustic solution was calculated in two stages. The time history of the pressure forces acting along the cylinder was calculated using a second order scheme and recorded during the LES run. Fast Fourier Transforms were then used in a post-processing stage to reach to the final result in Equ. (8).

HYDRODYNAMIC AND ACOUSTIC RESULTS

Simulations were carried for $Re_D=27\cdot10^3$ and $Fr_D=0.8$, of which there are some available hydrodynamic results, e.g. [2]. The computational domain height was 4*D* or 6*D* when the ambient water depth *h* was 2*D* or 4*D* respectively. This was found sufficient to counter any blockage effect in the air phase caused by the bow wave in front of the cylinder. A grid size of (129, 129, 71) points in the radial, tangential and vertical directions was used for the computational box of (20, 6)*D* in the radial and vertical directions. A similar resolution was used for the (20, 4)*D* computational domain. A much coarser grid was found to affect adversely the vortex shedding from the cylinder. The following results are inflow disturbance of a coherent asymmetric and synthetic turbulence, both with 2.5% amplitude as relative to the free stream velocity.

Typical instantaneous evolution of the interface surface for *h*=4*D* is shown in Figures 2, determined by the iso-surface of *C*=0.5. A bow wave with a maximum of height of about 0.3*D* is seen in front of the cylinder. The latter agrees well with the hydrodynamic head model that was found to predict well experimentally measured bow wave heights up to about $Fr_D=3$ [11]. The surface wake behind the cylinder shows the start of the Kelvin wake with about the well known 40^0 angle of opening, as well as the generation of short waves. The corresponding contours of the vorticity magnitude are also shown in Figures 2. It is seen that while the wake near the interface surface has

an overall symmetric structure, it changes to asymmetric with vortex rollers of Von Karman type as we get closer to the floor. Thus the interface surface attenuates asymmetric vortex shedding as was also found in [1] and [2].

The time history of the 2D lift coefficient C_l distribution along the cylinder is shown in Figures 3. Only the contribution of the water to the lift force is shown. As expected from the vortex shedding shown in Figures 2, C_l increases as it gets closer to the bottom floor, showing oscillations corresponding to about St_D=0.2, which is the fundamental frequency of vortex shedding in sub-critical single phase 2D circular cylinders [12]. The time-averaged value of C_d shown in Figures 3, varies between 0.85 to above 0.9, which is somewhat lower than the value for the single phase case of about 1.2 [12], but is less than 10% different than the value obtained in the free surface study in [2], supporting the opinion that the interface phase tends to reduce C_d. The distribution of Cl_{rms} shows a steady increase towards the floor but its maximum value is much lower than the single-phase value of about 0.35 (depending on inflow condition) and the value in [2] which varied between 0.2 to 0.4. Its distribution also differs from [2], which had a minimum around the mid plane between the free surface and the floor. However, it was found that by omitting the synthetic turbulence inflow condition and increasing the amplitude of the coherent disturbance to 5%, a distribution and values similar to those in [2] were recovered. This finding supports at least qualitatively the report in [12] for the single-phase case that increased upstream turbulence level can reduce Cl_{rms} and Cd_{rms} significantly.

A typical directivity distribution along the vertical direction is shown in Figures 4 using the hydrodynamic forces shown in Figures 3 for h=4D and similarly for h=2D. In both cases the directivity near the bottom floor peaks more or less around the stream-normal direction of θ=90^0 and 270^0, because of the vortex rollers and the dominance of C_l near the bottom. However, the latter was much weaker in the case of h=2D due to the damping effect of the interface surface resulting in a much earlier shift in the directivity towards the streamwise direction as one moves closer to the surface. The corresponding frequency spectra are shown in Figures 5. The cut-off frequency effect of the interface surface caused by its absorbing property is clear. For comparison, the frequency spectrum if the interface surface were totally reflecting is also plotted, showing a peak at the fundamental frequency of St_D=0.2 and that more than 40dB in the maximum level was lost for M=0.01. However for the radiative modes the loss was less than 5dB. It should be noted that M=0.01 corresponds to about 15m/s or 29 knots speed which is high for underwater applications. By equ. (7), h has to be higher than 1.25D/M in order for St_D=0.2 to become radiative. i.e. 125D for M=0.01. The vertical distribution of the frequency spectrum for M=0.02, shows as expected that the main contribution comes from the frequencies just above the cut-off frequency and near the bottom floor.

SUMMARY

The incompressible LES method based on a two-phase approach was coupled with a reformulated Lighthill-Curle acoustic analogy to investigate the sound generation and

propagation due to the interaction of free surface flow with vertically surface piercing cylinder, Both water and air phases were simulated with emphasis on the hydrodynamics and hydroacoustics occurring the water phase for a sub critical moderate Reynolds number and a moderate Froude number. Good qualitative and some quantitative agreements were found between the current hydrodynamic results and those reported in the literature. However, sensitivity to the inflow condition was found in the occurrence of vortex rollers and consequently in the fluctuation levels of the hydrodynamic force coefficients. Nevertheless, a general picture of a higher sound emission and propagation near the bottom floor was revealed.

The absorbing character of the interface surface was found to have a significant effect in damping low frequencies leaving only high frequency modes to propagate to the far field and thus reducing sufficiently the over far field acoustic power output, but only mildly damping the high frequency contribution. Further work is needed to verify the ability of the LES to capture that high frequency contribution. For example replacing the LES by the MILES approach based on a second order WENO scheme [13] proved to be more dissipative for the sound generation. Thus checking the effect of replacing the dissipative *Quick* scheme by a less dissipative and higher order scheme is a priority and a model for the direct contribution of the small scale structures to the sound emission should be investigated.

ACKNOWLEDGMENT

The authors wish to thank EPSRC for supporting this study and providing national computing time under grants GR/S46239/1 and EP/D044073/1

FIGURES

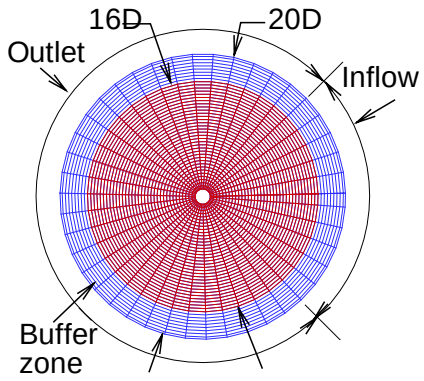

Figure 1: Schematic description of the cylindrical co-ordinates and the configurations of the inflow/outlet conditions. The inflow region covers an arc of 90^0.

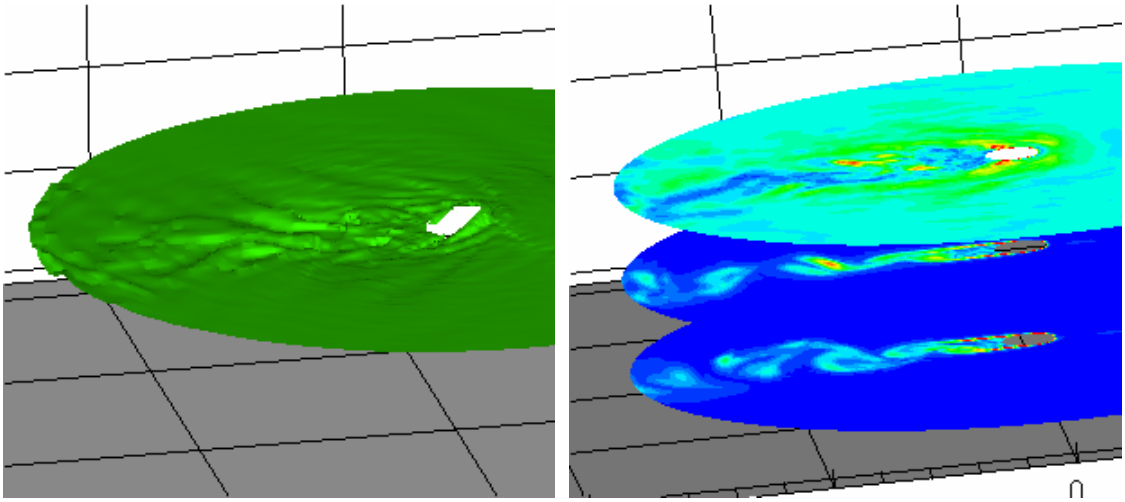

Figure 2: Instantaneous evolution of the interface surface (left) and the vorticity magnitude (right) at time 80, Re_D=27 10^3, Fr_D=0.8 and ambient water depth of 4*D*. The vorticity is plotted near the floor, 2*D* above it and close to the interface surface, with levels from 0.1 to 8.

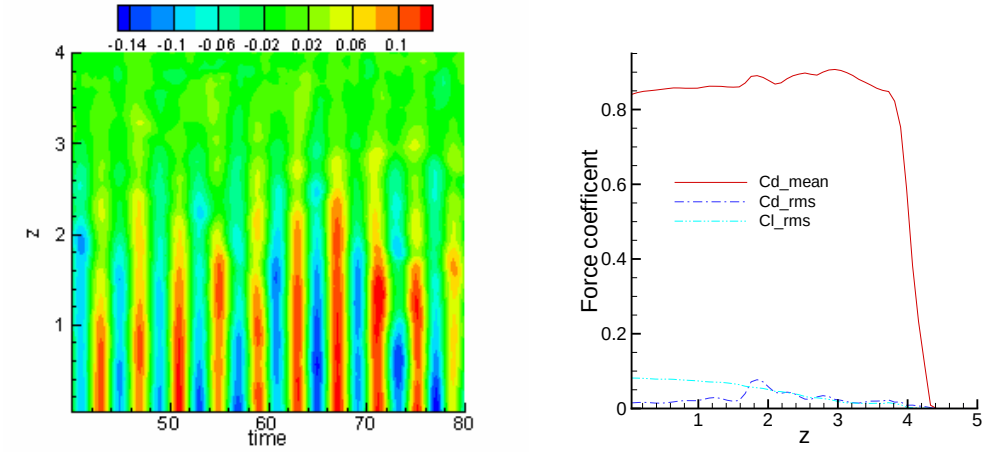

Figure 3: The time history of the lift coefficient C_l distribution along the cylinder (left) and the distribution of the time averaged and RMS of C_d and C_l along the cylinder (right) for the case of Figs. 2.

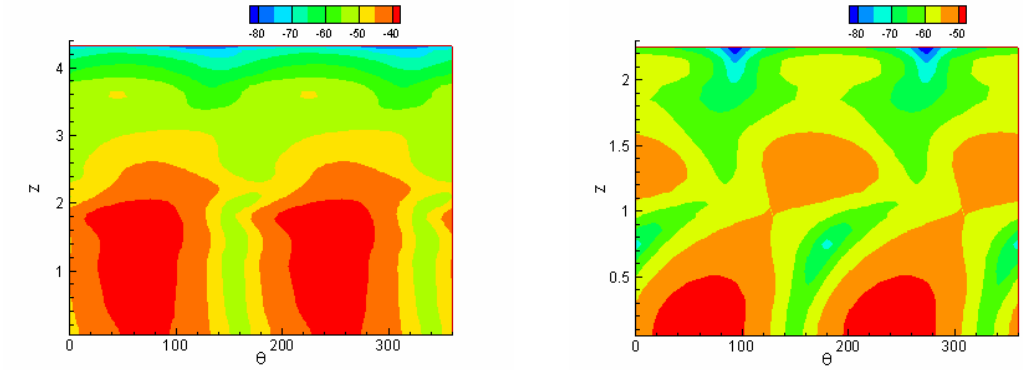

Figure 4: The far field directivity of the radiative modes for *M*=0.02 and ambient water depth of 4*D* (left), and 2*D* (right). Levels are in dB as results from the upstream mean flow

normalization. The rest of the conditions are as in Figure 2.

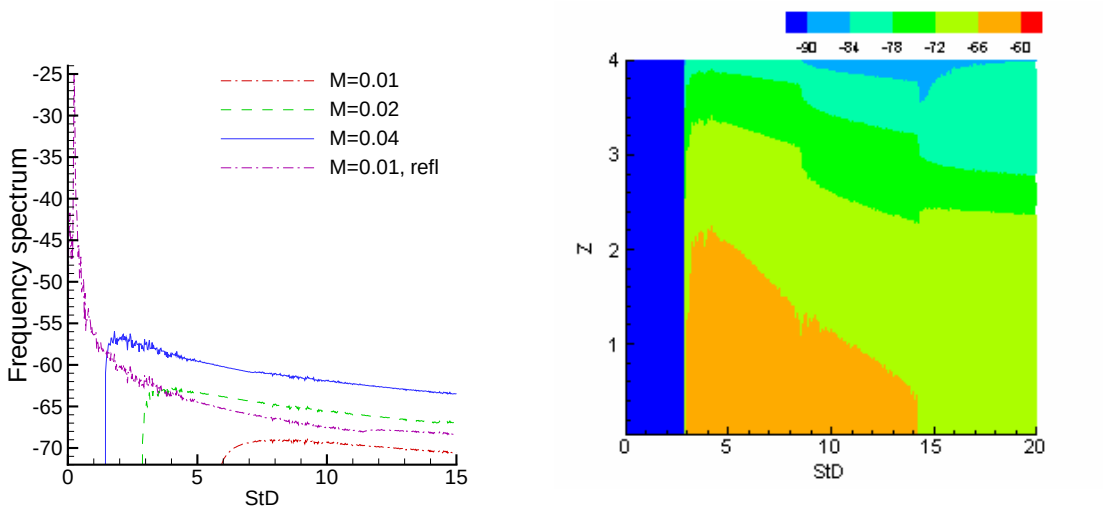

Figure 5: Frequency spectra for ambient water depth of 4*D*, showing the effect of the Mach number (left) and the vertical distribution for *M*=0.02 (right). Levels are in dB as in Figs 4

REFERENCES

[1] Innoue M., Baha N. and Himeno Y., "Experimental and numerical study of viscous flow around an advancing vertical circular cylinder piercing a free-surface", J. Kansai Soc. Naval Archit. Japan, **220**, 57-64 (1993).

[2] Kawamura T., Mayer S., Garapon A. and Sørensen L., "Large eddy simulation of a flow past a free surface piercing circular cylinder", J. Fluids Eng., **124**, 91-101 (2002).

[3] Powell A., "Theory of vortex sound", J. Acoust. Soc. Am., **36**, 177-195 (1964).

[4] Kato C., Iida A. and Ikegawa M., "Numerical simulation of aerodynamic sound radiated from low Mach number turbulent wakes", Proc. ASME/JSME Fluids Eng., **219**, 53-58 (1995)

[5] Yun G. and Choi H., "Prediction of sound from flow over circular cylinder using modified Green function", AIAA J., **42**(12), 2612-2615 (2004)

[6] Gloerfelt X., Pérot F., Bailly C. and Juvé D., "Flow-induced cylinder noise formulated as a diffraction problem for low Mach numbers", J. Sound Vib., **287**, 129-151 (2005)

[7] Saad Y, *Iterative Methods for Sparse Linear Systems*. SIAM, 2000.

[8] Rudman M., "Volume-tracking methods for interfacial flow calculations", Int J. Num. Meth. Fluids, **24**, 671-694 (1997)

[9] Li C.W. and Wang J.H., "Large eddy simulation of free surface shallow-water flow", Int J. Num. Meth. Fluids, **34**, 31-46 (2000)

[10] Howe MS, "Theory of vortex sound", Cambridge Press (2003)

[11] Wilkinson RH and Wickramasinghe D, "Wakes and waves generated by surface piercing cylinders", Report EX 3545, HR Wallingford (1996)

[12] Sumer BM and Fredsøe J., "Hydrodynamics around cylindrical structures", Advanced Series on Costal Eng. **12**, World Scientific (1999)

[13] Jiang G.S. and Shu C.W., "Efficient implementation of weighted ENO schemes", J. Comp. Phys. **126**, 202-228 (1996)